**Table 2.** Kinetic parameters for forward and reverse isomerization reactions. $k_{uncat}$, uncatalyzed reaction rate from (*32*); $^{app}K_{eq}$ (last column) is the apparent equilibrium constant [Haldane constant (*30*)] calculated from the ratio $k_{cat}/K_M$ values of the forward and reverse reactions measured at 25°C, 100 mM triethanolamine, pH 7.8 (*9*, *22*). nd, not determined. wtTIM, wild-type parameters from (*9*).

| Protein | DHAP → GAP | | | | DHAP ← GAP | | | | $^{app}K_{eq}$ |
|---|---|---|---|---|---|---|---|---|---|
| | $k^{cat}$ ($s^{-1}$) | $K_M$ ($\mu M$) | $k_{cat}/K_M$ ($M^{-1}s^{-1}$) | $k_{cat}/k_{uncat}$ | $k_{cat}$ ($s^{-1}$) | $K_M$ ($\mu M$) | $k_{cat}/K_M$ ($M^{-1}s^{-1}$) | $k_{cat}/k_{uncat}$ | |
| NovoTim | | | | | | | | | |
| 1.0 | 0.05 | 330 | $1.5 \times 10^2$ | $2.4 \times 10^5$ | nd | nd | nd | nd | nd |
| 1.2 | 0.1 | 180 | $5.6 \times 10^2$ | $5.0 \times 10^5$ | 0.8 | 92 | $8.6 \times 10^3$ | $1.8 \times 10^5$ | 15 |
| 1.2.1 | 0.18 | 140 | $1.4 \times 10^3$ | $9.0 \times 10^5$ | 1.5 | 85 | $1.7 \times 10^4$ | $3.4 \times 10^5$ | 12 |
| 1.2.2 | 0.14 | 165 | $8.2 \times 10^2$ | $7.0 \times 10^5$ | 1.2 | 89 | $1.4 \times 10^4$ | $2.7 \times 10^5$ | 17 |
| 1.2.3 | 0.17 | 100 | $1.8 \times 10^3$ | $8.5 \times 10^5$ | 1.2 | 103 | $1.2 \times 10^4$ | $2.7 \times 10^5$ | 7 |
| 1.2.4 | 0.11 | 105 | $1.0 \times 10^3$ | $5.5 \times 10^5$ | 1.1 | 51 | $2.1 \times 10^4$ | $2.5 \times 10^5$ | 21 |
| wtTIM | 487 | 1600 | $3.0 \times 10^5$ | $>1 \times 10^9$ | $4. \times 10^3$ | 390 | $1.0 \times 10^7$ | $1.0 \times 10^9$ | 33 |

anticipate that the design method will be extended to other substrates and reactions.

### References and Notes


1. R. Wolfenden, M. J. Snider, *Acc. Chem. Res.* **34**, 938 (2001).
2. S. J. Benkovic, S. Hammes-Schiffer, *Science* **301**, 1196 (2003).
3. M. Garcia-Viloca, J. Gao, M. Karplus, D. G. Truhlar, *Science* **303**, 186 (2004).
4. D. N. Bolon, C. A. Voigt, S. L. Mayo, *Curr. Opin. Chem. Biol.* **6**, 125 (2002).
5. D. Hilvert, *Annu. Rev. Biochem.* **69**, 751 (2000).
6. H. W. Hellinga, F. M. Richards, *J. Mol. Biol.* **222**, 763 (1991).
7. L. L. Looger, M. A. Dwyer, J. J. Smith, H. W. Hellinga, *Nature* **423**, 185 (2003).
8. S. L. Mowbray, L. B. Cole, *J. Mol. Biol.* **225**, 155 (1992).
9. J. R. Knowles, *Nature* **350**, 121 (1991).
10. D. G. Fraenkel, *Annu. Rev. Biochem.* **55**, 317 (1986).
11. J. P. Richard, T. L. Amyes, *Curr. Opin. Chem. Biol.* **5**, 626 (2001).
12. J. P. Richard, *Biochemistry* **24**, 949 (1985).
13. W. W. Cleland, P. A. Frey, J. A. Gerlt, *J. Biol. Chem.* **273**, 25529 (1998).
14. T. K. Harris, C. Abeygunawardana, A. S. Mildvan, *Biochemistry* **36**, 14661 (1997).
15. I. Kursula, R. K. Wierenga, *J. Biol. Chem.* **278**, 9544 (2003).
16. G. Jogl, S. Rozovsky, A. E. McDermott, L. Tong, *Proc. Natl. Acad. Sci. U.S.A.* **100**, 50 (2003).
17. E. Lolis, G. A. Petsko, *Biochemistry* **29**, 6619 (1990).
18. G. P. Ferguson, S. Totemeyer, M. J. MacLean, I. R. Booth, *Arch. Microbiol.* **170**, 209 (1998).
19. N. S. Sampson, J. R. Knowles, *Biochemistry* **31**, 8488 (1992).
20. M. S. Wisz, H. W. Hellinga, *Proteins* **51**, 360 (2003).
21. R. M. De Lorimier *et al.*, *Protein Sci.* **11**, 2655 (2002).
22. Information on materials and methods is available on *Science* Online.
23. M. A. Dwyer, L. L. Looger, H. W. Hellinga, *Proc. Natl. Acad. Sci. U.S.A.* **100**, 11255 (2003).
24. J. D. Hermes, S. M. Parekh, S. C. Blacklow, H. Koster, J. R. Knowles, *Gene* **84**, 143 (1989).
25. M. Zaccolo, D. M. Williams, D. M. Brown, E. Gherardi, *J. Mol. Biol.* **255**, 589 (1996).
26. R. T. Raines, E. L. Sutton, D. R. Straus, W. Gilbert, J. R. Knowles, *Biochemistry* **25**, 7142 (1986).
27. B. Kuhlman *et al.*, *Science* **302**, 1364 (2003).
28. J. A. Schellman, *Compt. Rend. Trav. Lab. Carlsberg Ser. Chim.* **29**, 230 (1955).
29. I. H. Segel, *Enzyme Kinetics* ( Wiley, New York, 1975).
30. A. Fersht, *Structure and Mechanism in Protein Science: A Guide to Enzyme Catalysis and Protein Folding* (Freeman, New York, 1999).
31. Single-letter abbreviations for the amino acid residues are as follows: A, Ala; C, Cys; D, Asp; E, Glu; F, Phe; G, Gly; H, His; I, Ile; K, Lys; L, Leu; M, Met; N, Asn; P, Pro; Q, Gln; R, Arg; S, Ser; T, Thr; V, Val; W, Trp; X, any amino acid; and Y, Tyr.
32. A. Hall, J. R. Knowles, *Biochemistry* **14**, 4348 (1975).


33. We thank G. Hammes, M. Allert, and K. Midelfort for insightful discussion and L. Loew for the gift of the styryl dyes. This work was supported by a grant to H.W.H. from the Defense Advanced Research Projects Agency.


**Supporting Online Material**

www.sciencemag.org/cgi/content/full/304/5679/1967/DC1
Materials and Methods
Figs. S1 to S4
Tables S1 and S2
References

29 March 2004; accepted 6 May 2004

# RNAi-Independent Heterochromatin Nucleation by the Stress-Activated ATF/CREB Family Proteins

**Songtao Jia, Ken-ichi Noma, Shiv I. S. Grewal***

**At the silent mating-type interval of fission yeast, the RNA interference (RNAi) machinery cooperates with *cenH*, a DNA element homologous to centromeric repeats, to initiate heterochromatin formation. However, in RNAi mutants, heterochromatin assembly can still occur at low efficiency. Here, we report that Atf1 and Pcr1, two ATF/CREB family proteins, act in a parallel mechanism to the RNAi pathway for heterochromatin nucleation. Deletion of *atf1* or *pcr1* alone has little effect on silencing at the mating-type region, but when combined with RNAi mutants, double mutants fail to nucleate heterochromatin assembly. Moreover, deletion of *atf1* or *pcr1* in combination with *cenH* deletion causes loss of silencing and heterochromatin formation. Furthermore, Atf1 and Pcr1 bind to the mating-type region and target histone H3 lysine-9 methylation and the Swi6 protein essential for heterochromatin assembly. These analyses link ATF/CREB family proteins, involved in cellular response to environmental stresses, to nucleation of constitutive heterochromatin.**

Heterochromatin governs diverse processes ranging from gene regulation and chromosome segregation to suppression of deleterious recombination in repetitive sequences. In the fission yeast *Schizosaccharomyces pombe*, heterochromatin is present mainly at the centromeres, telomeres, and a 20-kb silent domain at the mating-type region, the loci that are preferentially enriched in histone H3 lysine-9 (H3-K9) methylation and the Swi6 protein (a homolog of mammalian HP1 proteins) (*1*). The mechanisms that define these chromosomal regions as preferred sites of heterochromatin formation are not fully understood. Recent studies have implicated RNAi pathway in targeting of heterochromatin to repetitive DNA sequences in *S. pombe* and in other organisms including *Tetrahymena*, *Arabidopsis*, and *Drosophila* (*2*–*7*). It has been demonstrated that deletions of factors involved in the RNAi pathway such as Dicer (*dcr1*), RNA-dependent RNA polymerase (*rdp1*), and Argonaute (*ago1*) disrupt heterochromatin assembly at centromeres (*4*). Moreover, *cenH* sequence [96% similar to dg and dh centromeric repeats (*8*)] that is present at the silent mating-type (*mat2/3*) region (see Fig. 1A) serves as an RNAi-dependent heterochromatin nucleation center at the endogenous locus and at an ectopic location (*2*). Although RNAi

machinery cooperates with *cenH* to initiate heterochromatin formation at the *mat2/3* region, the RNAi pathway is dispensable for the subsequent maintenance of heterochromatin at this locus (*2*). Moreover, deletion of *cenH* causes specific defects in the establishment of the silenced state. In strains where *cenH* is replaced with the *ura4*$^+$ reporter gene (*KΔ::ura4*$^+$), cells carrying an *ura4-on* epigenetic state switch to the *ura4-off* epigenetic state inefficiently; however, once established, the *ura4-off* state is stably inherited and rarely switches back to the *ura4-on* state (*8*). This establishment of the silenced state is coupled to H3-K9 methylation and Swi6 recruitment at the *mat2/3* region (*9*). Furthermore, Swi6 overexpression can efficiently convert the *ura4-on* state to the *ura4-off* state, which suggests that Swi6 can cooperate with elements outside of *cenH* to nucleate heterochromatin assembly independent of RNAi.

We hypothesized that the RNAi-independent pathway of heterochromatin nucleation might involve factors that localize to specific site(s) within the *mat2/3*

Laboratory of Molecular Cell Biology, National Cancer Institute, National Institutes of Health, Bethesda, MD 20892, USA.

*To whom correspondence should be addressed. E-mail: grewals@mail.nih.gov

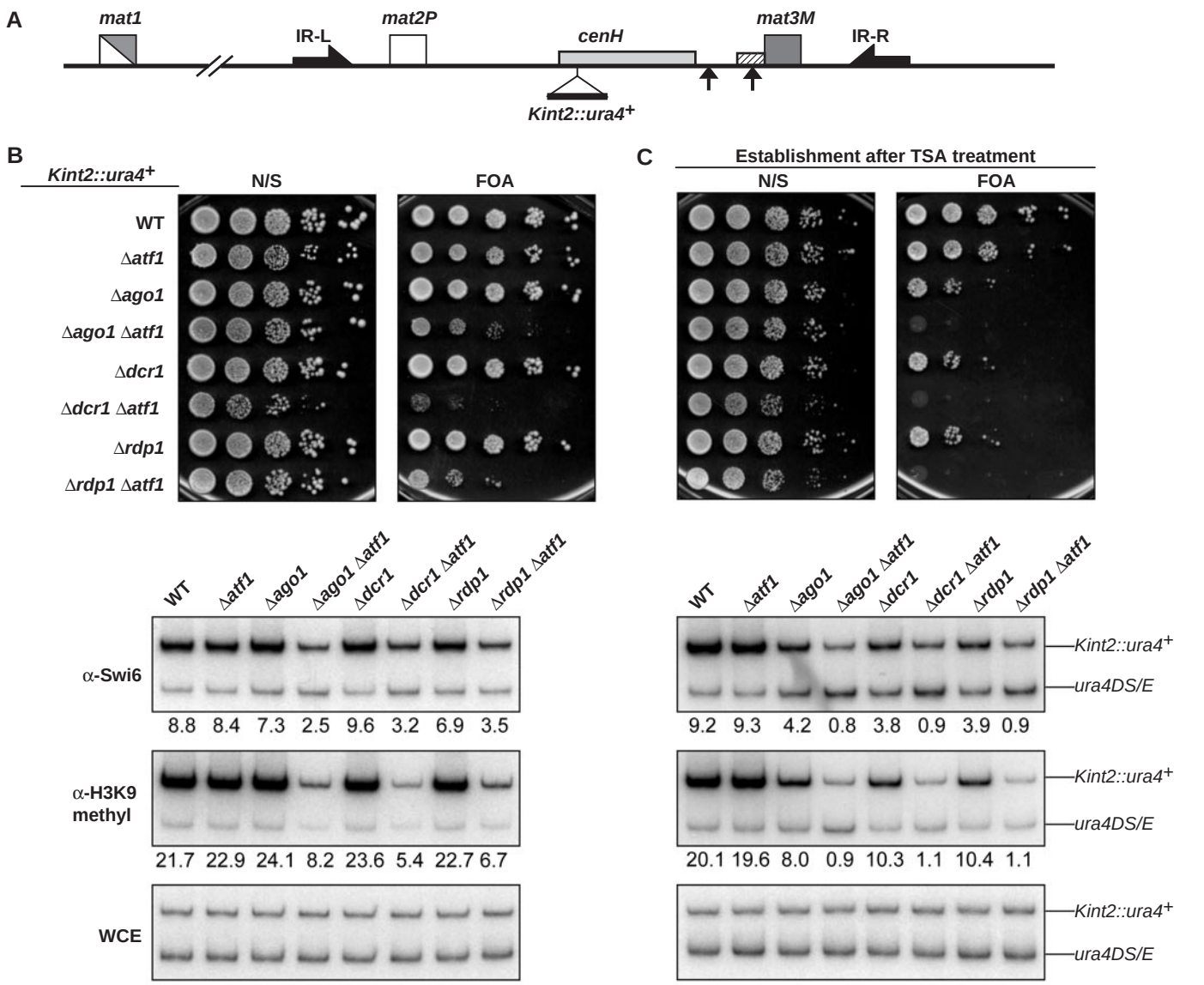


**Fig. 1.** Atf1 is required for heterochromatin formation at the silent mating-type region. (**A**) A schematic diagram of the mating-type region. Black arrows represent IR-L and IR-R boundary elements. Shaded box denotes *cenH* sequence and striped box represents *REIII* sequence. Arrowheads indicate binding sites for Atf1/Pcr1. (**B**) △*atf1* in combination with RNAi mutants affect maintenance of heterochromatin at *Kint2::ura4*$^+$. Serial dilution plating assays in the presence and absence of FOA were performed to measure *Kint2::ura4*$^+$ expression. Levels of Swi6 and H3-K9 methylation at *Kint2::ura4*$^+$ were determined by ChIP. DNA isolated from immunoprecipitated chromatin fractions or from whole-cell extract (WCE) was quantitatively analyzed by competitive polymerase chain reaction (PCR), in which one primer pair amplifies different-sized PCR products from the *Kint2::ura4*$^+$ and the control *ura4DS/E* minigene at the endogenous location. The ratios of intensities of *ura4*$^+$ to *ura4DS/E* signals in the ChIP and WCE lanes were used to calculate the relative fold enrichment, shown below each lane. (**C**) △*atf1* in combination with RNAi mutants completely abolished the establishment of heterochromatin. Cells were grown in medium containing 35 μg/ml TSA for 10 generations and were allowed to recover in the absence of TSA for an additional 10 generations. Expression of *Kint2::ura4*$^+$ and levels of Swi6 and H3-K9 methylation at *Kint2::ura4*$^+$ after recovery from TSA treatment are shown.

region and could act upstream of H3-K9 methylation and Swi6 localization. In a *swi6* mutant, H3-K9 methylation is asymmetrically enriched around the *cenH* repeat with more methylation on the *mat3* side of the *cenH* locus (*2*), which suggests that unknown factors binding between *cenH* and *mat3* may function to recruit heterochromatin. Analysis of a 2.1-kb region between *cenH* and the *mat3* loci revealed two heptamer sequences ATGACGT, a well-characterized binding site for the transcription factor Atf1/Pcr1 (*10*). One of these sites overlaps with a silencer element involved in Swi6-independent local repression of the *mat3* locus (*10*).

Both Atf1 and Pcr1 contain a bZIP DNA binding domain that shares strong homology with the activating transcription factor/cAMP response element–binding protein (ATF/CREB) family of proteins and they regulate gene expression during sexual differentiation and environmental stress (*11*–*13*). To determine whether Atf1 and Pcr1 are involved in heterochromatin formation at the silent mating-type region, we generated *atf1* and *pcr1* deletion strains carrying a *Kint2::ura4*$^+$ reporter (see Fig. 1A). Deletion of either of these factors had little effect on the maintenance of heterochromatin at this region (Figs. 1B and 2A). However, when *aft1* or *pcr1* deletion was combined with RNAi mutants, we observed a striking decrease in the silencing of the *ura4*$^+$ reporter, which correlated with significant reduction in histone H3-K9 methylation levels and Swi6 localization (Figs. 1B and 2A). We also investigated the effect of these mutations on the initial establishment of heterochromatin at the *mat2/3* region. Treatment of cells with the histone deacetylase inhibitor trichostatin A (TSA) is known to derepress the mating-type region; however, silencing is efficiently reestablished once cells are allowed to recover in the absence of the drug (*2*). In contrast, in *ago1*, *dcr1*, or *rdp1* mutants, reestablishment of the silent state after TSA treatment is impaired, although heterochromatin formation still occurred at a slower rate (Figs. 1C and 2B) (*2*). When deletion of RNAi components was combined with either △*atf1* or △*pcr1*, double mutants strikingly failed to reestablish silencing, which was coupled with complete loss of H3-K9 methylation and the Swi6 protein at the *mat* locus (Figs. 1C and 2B). The residual silencing observed in double mutants before TSA treatment could reflect the ability of heterochromatin complexes to promote their own reassembly in the absence of de novo nucleation (*9*). Taken together, these results demonstrate that Atf1/Pcr1 and RNAi machinery act in parallel

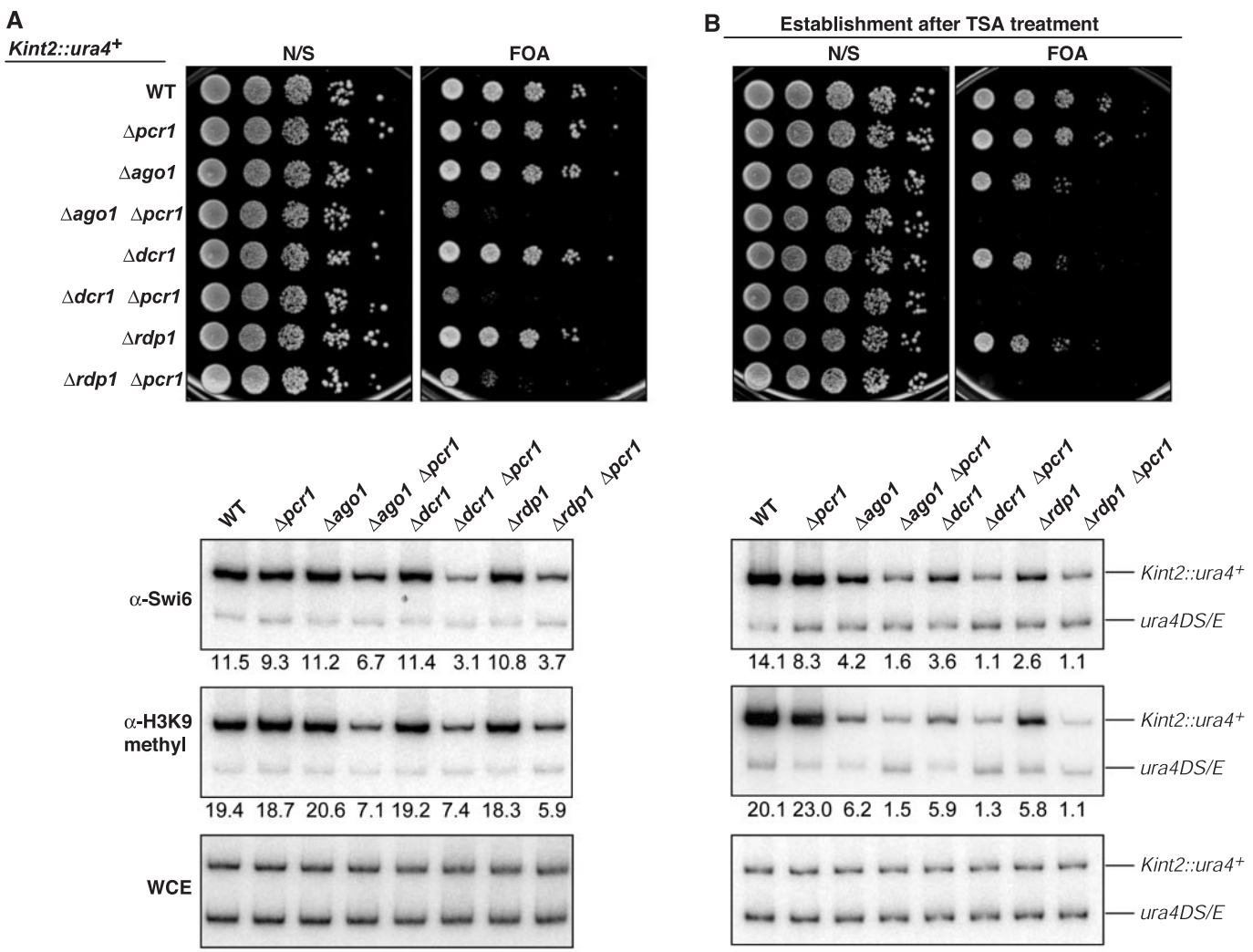


**Fig. 2.** Pcr1 is required for heterochromatin formation at the silent mating-type region. (**A**) △*pcr1* in combination with RNAi mutants affect heterochromatin at *Kint2::ura4*$^+$. Expression of *ura4*$^+$ and levels of Swi6 and H3-K9 methylation at *Kint2::ura4*$^+$ are shown. (**B**) △*pcr1* in combination with RNAi mutants completely abolished the establishment of heterochromatin. Cells were treated with TSA as described in Fig. 1C. Expression of *ura4*$^+$ and levels of Swi6 and H3-K9 methylation at *Kint2::ura4*$^+$ after recovery from TSA treatment are shown.

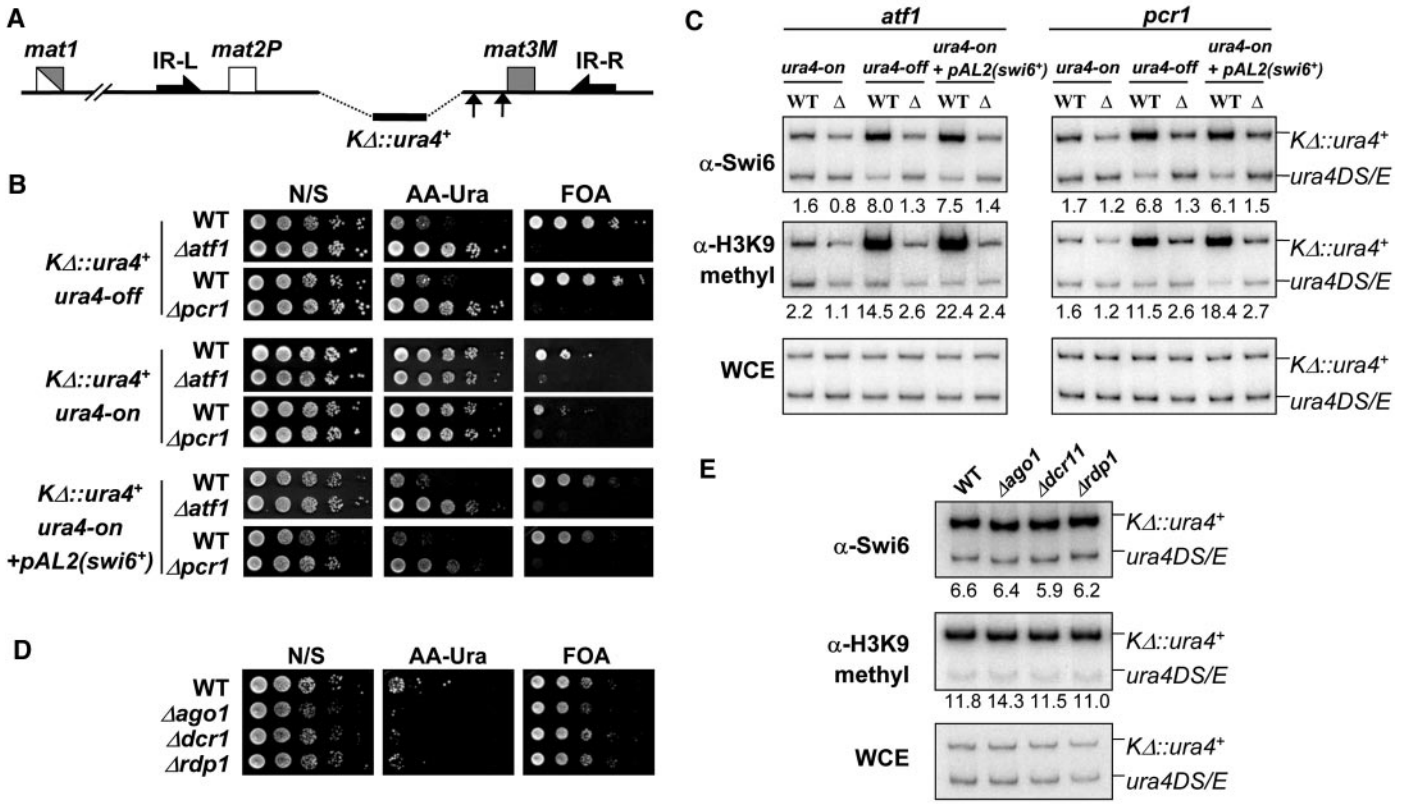


**Fig. 3.** *atf1* and *pcr1* act in a redundant manner as the RNAi pathway to silence the *mat2/3* region. (**A**) Schematic diagram of the *mat* locus in *KΔ::ura4*$^+$ strain carrying the replacement of the *cenH* with *ura4*$^+$. (**B**) *KΔ::ura4*$^+$ marker showing the *ura4-off* or the *ura4-on* state was combined with △*atf1* or △*pcr1* and serial dilution plating assay was used to measure *ura4*$^+$ expression. (**C**) Levels of Swi6 and H3-K9 methylation at *KΔ::ura4*$^+$ were determined by ChIP. (**D**) *KΔ::ura4*$^+$ *ura4-off* epiallele was combined with mutations in RNAi components and expression of *ura4*$^+$ was measured using serial dilution plating assay. (**E**) Levels of Swi6 and H3-K9 methylation at *KΔ::ura4*$^+$ determined by ChIP.

pathways to nucleate heterochromatin formation at the *mat2/3* region.

In support of these findings, deletion of either *atf1* or *pcr1*, but not RNAi mutants, in combination with *cenH* deletion (Fig. 3A) resulted in loss of silencing and heterochromatin assembly at the *mat2/3* locus. As shown in Fig. 3B (top), deletion of *aft1* or *pcr1* in the *KΔ::ura4*$^+$ strain resulted in the efficient conversion of the *ura4-off* state to the *ura4-on* state. This change was accompanied by loss of H3-K9 methylation and Swi6 localization at the *mat* locus (Fig. 3C). Moreover, △*atf1* or △*pcr1* inhibited the stochastic conversion of the *ura4-on* state to the *ura4-off* state (Fig. 3B, middle). In contrast, RNAi mutants combined with *KΔ::ura4*$^+$ *ura4-off* epiallele had no effect on silencing, H3-K9 methylation, or Swi6 localization at the *mat2/3* region (Fig. 3, D and E). Therefore, we conclude that *cenH* and RNAi machinery function in the same pathway to silence the *mat* locus. Cells that lack this heterochromatin assembly pathway rely completely on a second pathway mediated by Atf1/Pcr1.

To investigate whether Swi6-induced establishment of silencing in the absence of *cenH* (*9*) requires Atf1/Pcr1, *KΔ::ura4*$^+$ *ura4-on* cells were transformed with a plasmid carrying the *swi6*$^+$ gene. Unlike wild-type background cells, Swi6 overexpression in △*atf1* or △*pcr1* strains failed to convert the *ura4-on* to the *ura4-off* state (Fig. 3B, bottom) and no detectable increases in H3-K9 methylation or the Swi6 protein were observed at the *mat* locus (Fig. 3C). These data demonstrate that in the absence of RNAi, Atf1 and Pcr1 are indispensable for heterochromatin nucleation at the *mat2/3* region and that they may participate in the creation of a second nucleation site for heterochromatin formation. To test this idea, a strain carrying deletion of one of the Atf1/Pcr1-binding sites (△*REIII*) at the *mat2/3* region was constructed together with a *Kint2::ura4*$^+$ reporter (Fig. 1A) (*10*). As expected, deletions of RNAi components in combination with △*REIII* greatly reduced establishment of silencing of *Kint2::ura4*$^+$ after TSA treatment (Fig. 4A), concurrent with dramatic reduction of H3-K9 methylation and the Swi6 protein at the *mat2/3* region when compared with either single mutants or a wild-type strain (Fig. 4A).

We next tested whether Atf1 and Pcr1 bind directly to their putative binding sites in vivo. Indeed, mapping of Atf1 and Pcr1 by chromatin immunoprecipitation (ChIP) revealed that both proteins specifically localize to regions containing their binding sites and that no binding was detected at surrounding *mat2/3* sequences (Fig. 4B). Note that the localization of Atf1/Pcr1 to the *mat* locus was not dependent on the Swi6 protein (Fig. 4B). These findings suggest that Atf1/Pcr1 function upstream of Swi6 and could directly recruit heterochromatin machinery to the mating-type region.

Collectively, these data indicate that binding of Atf1/Pcr1 to their recognition sequences in the mating-type region creates a nucleation site for constitutive heterochromatic structures. To explore the mechanism of Atf1/Pcr1-mediated heterochromatin formation, we examined whether Atf1/Pcr1 could directly recruit factors involved in heterochromatin formation. We found that Atf1 or Pcr1 bind to the Swi6 and Clr4 proteins (Fig. 4C), consistent with our observation that Swi6-induced establishment of silencing requires Atf1/Pcr1 (Fig. 3B). This mechanism may resemble the recruitment of facultative het-

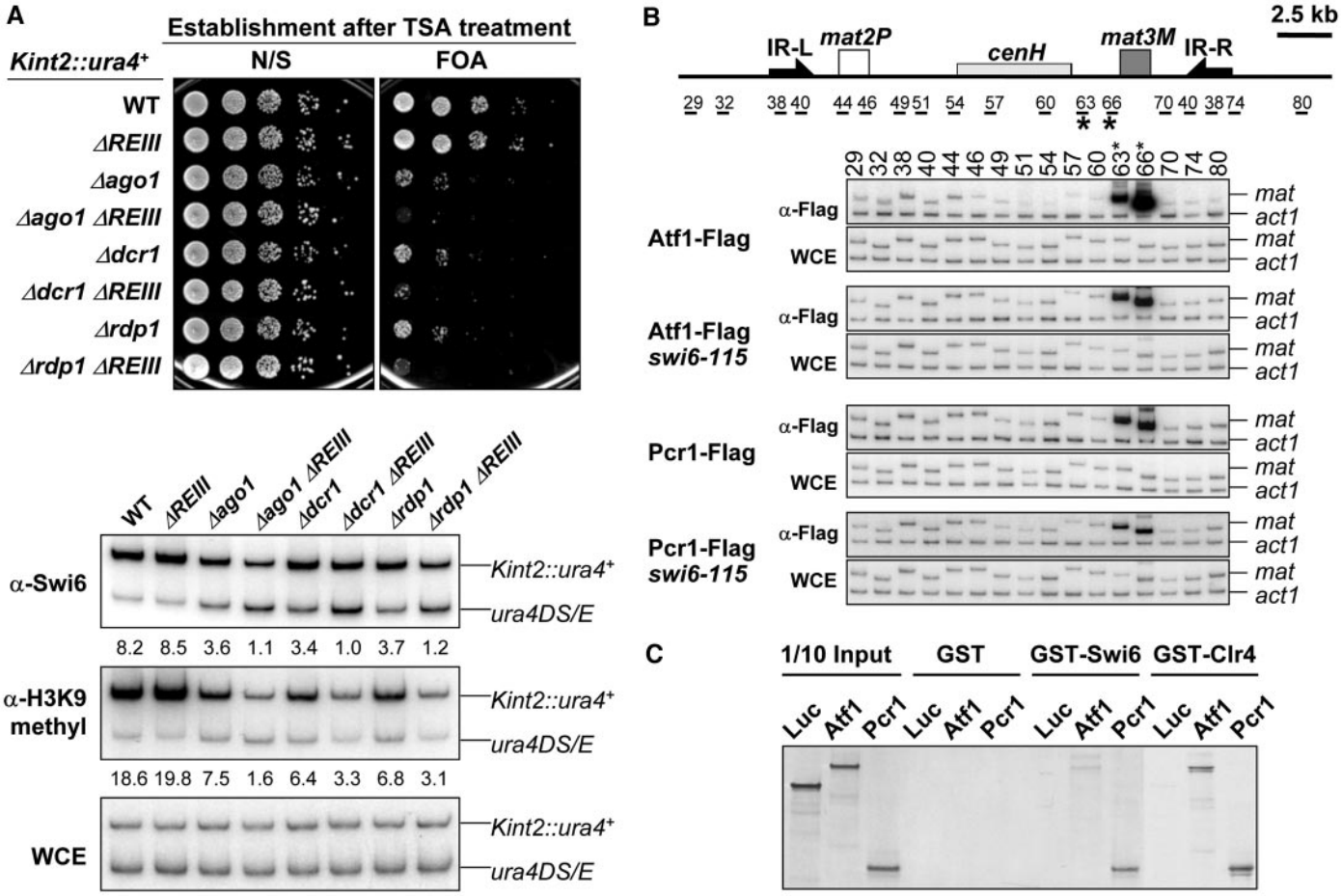


**Fig. 4.** *REIII* sequence containing Atf1/Pcr1-binding site is required for heterochromatin formation at the *mat2/3* region. (**A**) Effect of △*REIII* on heterochromatin nucleation in combination with RNAi mutants. Cells were treated with TSA as in Fig. 1C. Expression of *Kint2::ura4*$^+$ and levels of Swi6 and H3-K9 methylation at *Kint2::ura4*$^+$ after recovery from TSA treatment are shown. (**B**) High-resolution mapping of Atf1 and Pcr1 at the mating-type region. Strains expressing Atf1 and Pcr1 tagged with 3× FLAG (the DYDDDK epitope) were used to perform ChIP with FLAG-specific antibody. DNA isolated from ChIP or WCE fractions was subjected to multiplex PCR to amplify DNA fragments from the *mat* locus (indicated below the scheme at the top), as well as an *act1* control fragment. Asterisks indicate DNA fragments that contain Atf1/Pcr1-binding sites. (**C**) Atf1 and Pcr1 interact with Swi6 and Clr4. In vitro translated and $^{35}$S-labeled luciferase (Luc), Atf1, and Pcr1 were incubated with equal amounts of glutathione *S*-transferase (GST), GST-Swi6, or GST-Clr4 immobilized on glutathione beads and washed extensively. The eluted proteins were resolved by SDS–polyacrylamide gel electrophoresis and imaged by autoradiography.

erochromatin by KRAB/KAP-1 or retinoblastoma (Rb) protein in mammals, which can recruit histone modifying activities and heterochromatin proteins such as HP1 to silence specific genes located in otherwise euchromatic territories (*14*–*16*). It should be noted however that, unlike Rb or KRAB/KAP-1, Atf1/Pcr1-mediated constitutive heterochromatin spreads throughout the silent mating-type interval and this causes regional silencing.

The involvement of factors required for the cellular response to environmental stress in heterochromatin assembly suggests the possibility that these factors might modify chromatin structure as a part of a programmed sequence of events that serves to cushion against the effects of environmental stresses (*17*). In this respect, it is notable that Atf1 activity is regulated by Sty1/Spc1 protein kinases in response to environmental stress (*18*), and defects in heterochromatin assembly under elevated temperature conditions have been observed in different systems (*19*–*22*). In mammals, heat shock can also trigger the loss of heterochromatin structures at pericentric regions and elevates transcription of embedded satellite III repeat sequences (*23*). Considering the importance of heterochromatin in diverse cellular functions such as gene silencing, genome stability, and chromosome segregation, it is not surprising that cells have evolved multiple pathways of heterochromatin assembly.

### References and Notes


1. S. I. Grewal, *J. Cell. Physiol.* **184**, 311 (2000).
2. I. M. Hall *et al.*, *Science* **297**, 2232 (2002).
3. A. Verdel *et al.*, *Science* **303**, 672 (2004).
4. T. A. Volpe *et al.*, *Science* **297**, 1833 (2002).
5. K. Mochizuki, N. A. Fine, T. Fujisawa, M. A. Gorovsky, *Cell* **110**, 689 (2002).
6. D. Zilberman, X. Cao, S. E. Jacobsen, *Science* **299**, 716 (2003).
7. M. Pal-Bhadra *et al.*, *Science* **303**, 669 (2004).
8. S. I. Grewal, A. J. Klar, *Genetics* **146**, 1221 (1997).
9. J. Nakayama, A. J. Klar, S. I. Grewal, *Cell* **101**, 307 (2000).
10. G. Thon, K. P. Bjerling, I. S. Nielsen, *Genetics* **151**, 945 (1999).
11. T. Takeda *et al.*, *EMBO J.* **14**, 6193 (1995).
12. M. G. Wilkinson *et al.*, *Genes Dev.* **10**, 2289 (1996).
13. Y. Watanabe, M. Yamamoto, *Mol. Cell. Biol.* **16**, 704 (1996).
14. M. Lechner, G. Begg, D. Speicher, F. J. Rauscher III, *Mol. Cell. Biol.* **20**, 6449 (2000).
15. D. C. Schultz, K. Ayyanathan, D. Negorev, G. G. Maul, F. J. Rauscher III, *Genes Dev.* **16**, 919 (2002).
16. S. J. Nielsen *et al.*, *Nature* **412**, 561 (2001).
17. B. McClintock, *Science* **226**, 792 (1984).
18. G. Degols, P. Russell, *Mol. Cell. Biol.* **17**, 3356 (1997).
19. J. W. Gowen, E. H. Gay, *Science* **77**, 312 (1933).
20. J. B. Spofford, in *The Genetics and Biology of Drosophila*, M. Ashburner, E. Nivitski, Eds. (Academic Press, New York, 1976), pp. 955–1018.
21. R. C. Allshire, E. R. Nimmo, K. Ekwall, J. P. Javerzat, G. Cranston, *Genes Dev.* **9**, 218 (1995).

22. N. Ayoub, I. Goldshmidt, A. Cohen, *Genetics* **152**, 495 (1999).
23. N. Rizzi *et al.*, *Mol. Biol. Cell* **15**, 543 (2004).
24. We thank J. Rice and H. Cam for critical reading of the manuscript and members of the Grewal laboratory for helpful discussions. This work is funded by the National Cancer Institute.

**Supporting Online Material**
www.sciencemag.org/cgi/content/full/304/5679/1971/DC1
Materials and Methods
Table S1
References and Notes

24 February 2004; accepted 21 May 2004

# Postnatal Refinement of Peripheral Olfactory Projections

**Dong-Jing Zou,[1]* Paul Feinstein,[2] Aimée L. Rivers,[1] Glennis A. Mathews,[1] Ann Kim,[1] Charles A. Greer,[3] Peter Mombaerts,[2] Stuart Firestein[1]***

**Axonal projections from the olfactory epithelium to the olfactory bulb are organized into glomeruli according to the expressed odorant receptor. Using gene-targeted mice, we show that glomerular maturation proceeds along different time courses for two similar receptors and requires sensory input during distinct sensitive periods. During early development, some glomeruli are innervated by axons of neurons that do not express the same receptor. These heterogeneous glomeruli normally disappear with age, but they persist in adults deprived of sensory input by unilateral and permanent naris closure. Persistence may be due, in part, to prolonged survival of olfactory sensory neurons.**

The decoding of environmental stimuli detected by specialized sensory cells requires the formation of precise projections from the periphery to the brain. In mammalian olfactory systems, the connection between periphery and brain occurs over a single synapse. The axons of olfactory sensory neurons (OSNs) expressing the same odorant receptor (OR) project to spatially conserved regions of the olfactory bulb, where they coalesce into glomeruli (*1*–*5*). This process uses molecular determinants, but it remains controversial to what extent it also relies on sensory activity (*6*–*11*).

We examined the postnatal formation of glomeruli for ORs M71 and M72 in gene-targeted M71-IRES-taulacZ and M72-IRES-taulacZ mice (M71 and M72 mice) during development (*12*, *13*). The expression of the axonal marker tau–β-galactosidase (β-gal) encoded by the gene taulacZ is under the direct control of the endogenous M71 or M72 OR promoter (*8*, *14*, *15*). ORs M71 and M72 are highly homologous, with 96% identity in their amino acid sequences. The axons from OSNs expressing these ORs (referred to as M71 or M72 axons) each form at least one medial and one lateral glomerulus (M71 or M72 glomerulus) in adult olfactory bulbs. M71 and M72 glomeruli are located within a few hundred microns of each other.

The positions of specific glomeruli are bilaterally symmetrical between olfactory bulbs, each of which possesses an internal symmetry as well. There are thus four "half-bulbs" in an individual. In newborn mice (Postnatal Day 0, PD0), M71 and M72 axons had reached two spatially conserved posterior-dorsal areas in each bulb (one each on the medial and lateral half-bulbs), but the axons were widely scattered, and M71 and M72 glomeruli were not yet identifiable (*8*, *16*). By PD10 these glomeruli were clearly defined, but there were often multiple M71 and M72 glomeruli at either the medial or lateral half-bulbs (whole-mount observations, Fig. 1A), whose precise locations varied within a spatially conserved region. In older animals (≥PD40), single M71 and M72 glomeruli were generally observed in both the medial and lateral half-bulbs (Fig. 1, B and C). Between PD10 and PD60, the proportion of half-bulbs with multiple glomeruli decreased significantly [$P < 0.01$ (*17*)] from 52% (M71, $n = 112$) to 16% ($n = 80$) and from 55% (M72, $n = 88$) to 17% ($n = 76$), with a corresponding increase in single glomeruli (Fig. 1D). These observations suggest a process of OSN axon projection refinement, which may reflect a threshold of an axonal population needed to maintain a glomerulus (*18*).

M71 and M72 glomeruli matured differently (Fig. 1E). M71 glomeruli underwent a prolonged maturation, and the average number of M71 glomeruli per half-bulb did not reach the mature level (>PD90) until PD60. In contrast, the average number of M72 glomeruli per half-bulb rapidly decreased to the level of mature animals (>PD90) by PD20. Thus, glomerular maturation can follow distinct time courses for even closely related ORs.

A hallmark of mature glomeruli is that they are innervated exclusively by axons from OSNs expressing the same OR (*5*). To establish whether this is the case for glomeruli in young animals, we used a double-label immunohistochemical protocol on serial coronal cryosections with antibodies for olfactory marker protein (OMP) to stain all mature OSN axons, and antibodies for β-gal to label M71 (or M72) axons. In homogeneous M71 (or M72) glomeruli, immunoreactivity for these two markers should largely overlap. At PD10, when multiple glomeruli are commonly observed in each half-bulb, most M71 (or M72) glomeruli exhibited colocalization of OMP and β-gal immunoreactivity (Fig. 2A and Table 1). But many M71 and M72 glomeruli also exhibited OMP-positive, β-gal–negative axons (Fig. 2B and Table 1), suggesting that these immature glomeruli are innervated also by axons from OSNs expressing other ORs. In contrast, in PD60 animals,

**Table 1.** Homogeneous and heterogeneous glomeruli during development and after naris closure. The organization of OSN axons within M71 and M72 glomeruli was examined by OMP and β-gal double immunostaining in serial coronal sections through the bulbs of both normally developed and naris-closed animals. Animals were naris closed at PD0 to PD5 (M71) or PD0 (M72) and examined at PD40.

| Glomeruli | Age/side | Number of half-bulbs | Total glomeruli per half-bulb (min–max) | Homogeneous glomeruli per half-bulb | Heterogeneous glomeruli per half-bulb |
|---|---|---|---|---|---|
| | | | Normally developed animals | | |
| M71 | PD10 | 18 | 1.78 ± 0.26 (1–5) | 1.33 ± 0.14 | 0.44 ± 0.25 |
| | PD60 | 14 | 1.29 ± 0.13 (1–2) | 1.21 ± 0.15 | 0.07 ± 0.07 |
| M72 | PD10 | 16 | 1.81 ± 0.21* (1–3) | 1.19 ± 0.19 | 0.63 ± 0.18* |
| | PD60 | 18 | 1.11 ± 0.08 (1–2) | 0.94 ± 0.10 | 0.17 ± 0.09 |
| | | | Naris-closed animals | | |
| M71 | closed | 14 | 2.43 ± 0.17† (2–4) | 1.14 ± 0.15 | 1.29 ± 0.19† |
| | open | 14 | 1.07 ± 0.07 (1–2) | 0.93 ± 0.07 | 0.14 ± 0.14 |
| M72 | closed | 12 | 2.25 ± 0.13† (2–3) | 0.92 ± 0.19 | 1.33 ± 0.19† |
| | open | 12 | 1.33 ± 0.19 (1–3) | 1.17 ± 0.21 | 0.17 ± 0.17 |

Statistically significant ($P < 0.05$, run on SPSS program): *Comparing normally developed animals between PD10 and PD60, Mann-Whitney test. †Comparing naris-closed animals between bulb$^X$ and bulb$^O$, Wilcoxon signed-ranks test.

[1]Department of Biological Sciences, Columbia University, New York, NY 10027, USA. [2]The Rockefeller University, New York, NY 10021, USA. [3]Departments of Neurosurgery and Neurobiology, Yale University School of Medicine, New Haven, CT 06520, USA.

*To whom correspondence should be addressed. E-mail: dz98@columbia.edu (D.-J.Z.); sjf24@columbia.edu (S.F.)